frontiers in Environmental Chemistry

ORIGINAL RESEARCH
published: 13 May 2021
doi: 10.3389/fenvc.2021.672844

The Strategy for Constructing the Structure: Pt-O-Ce^{3+} Applied in Efficient NO_X Removal

Guoquan Liu[1†], Zhifei Hao[1†], Xueyue Mi[1], Nan Ma[1], He Zhang[1], Yi Li[2] and Sihui Zhan[1]*

[1] Ministry of Education Key Laboratory of Pollution Processes and Environmental Criteria, Tianjin Key Laboratory of Environmental Remediation and Pollution Control, College of Environmental Science and Engineering, Nankai University, Tianjin, China, [2] Tianjin Key Laboratory of Molecular Optoelectronic Sciences, Department of Chemistry, Collaborative Innovation Center of Chemical Science and Engineering, School of Science, Tianjin University, Tianjin, China

Exploring a unique structure with superior catalytic performance has remained a severe challenge in many important catalytic reactions. Here, we reported a phenomenon that CeO_2-based catalysts loaded with different Pt precursors showed a significant difference in the performance of the reduction of NO with H_2. The supported platinum nitrate [PtCe(N)] exhibited a superior low-temperature catalytic performance than the supported chloroplatinic acid [PtCe(C)]. In a wide operating temperature (125–200°C), more than 80% NO_x conversion was achieved over PtCe(N) as well as excellent thermal stability. Various characterizations were used to study the microstructure and chemical electronic states. Results showed the introduction of a low valence state of Pt species into the CeO_2 resulted in the rearrangement of charges on the surface of CeO_2, accompanied by increasing contents of oxygen vacancies and Ce^{3+} sites. Furthermore, the X-ray photoelectron spectroscopy (XPS) and Raman spectra confirmed that the divalent Pt atom could substitute Ce atom to form the Pt-O-Ce^{3+} structure, which was the base unit in the high-performance PtCe(N) catalyst. The tunable catalytic system of the Pt-O-Ce^{3+} structure provides a strategy for the design of supported metal catalysts and may as a model unit for future studies of many other reactions.

Keywords: NO_x removal, oxygen vacancy, Ce^{3+} site, Pt-O-Ce^{3+}, substitution

OPEN ACCESS

Edited by:
Dengsong Zhang,
Shanghai University, China

Reviewed by:
Zhiming Liu,
Beijing University of Chemical Technology, China
Jian-Wen Shi,
Xi'an Jiaotong University, China

****Correspondence:***
Sihui Zhan
sihuizhan@nankai.edu.cn

† These authors have contributed equally to this work

Specialty section:
This article was submitted to Catalytic Remediation, a section of the journal Frontiers in Environmental Chemistry

Received: *26 February 2021*
Accepted: *01 April 2021*
Published: *13 May 2021*

Citation:
Liu G, Hao Z, Mi X, Ma N, Zhang H, Li Y and Zhan S (2021) The Strategy for Constructing the Structure: Pt-O-Ce^{3+} Applied in Efficient NO_x Removal. Front. Environ. Chem. 2:672844. doi: 10.3389/fenvc.2021.672844

INTRODUCTION

The use and application of diesel engines in industrial processes became widespread due to their good power performance and economy (Pronk et al., 2009). Excessive emission of nitrogen oxides (NO_x) can cause serious environmental pollution and severe health issues (Anenberg et al., 2017; Oberschelp et al., 2019). For example, photochemical smog and acid rain were caused by the high toxicity of NO_x. Meanwhile, NO_x can also damage the lungs and cause respiratory diseases (Han et al., 2019b). Because of the series of hazards, several measures were used to eliminate the effects of NO_x emission. Periodic operation in dilute and concentrated combustion phases was applied in NO_x storage and reduction (NSR) technology to prevent pollution (Yoshida et al., 2016). A non-negligible amount of reductive gas (H_2, HC, and CO) was generated during the rich regeneration period of the diesel lean NO_x trap. In addition, H_2 molecules still tended toward high activity even

at low temperatures and after the catalysts were aged, so that the reduction of NO with H_2 as the model was mentioned by researchers (Abdulhamid et al., 2003; Jozsa et al., 2004). Compared to traditional NH_3-SCR reaction, H_2 as the reductant has advantages of lower temperature activity, cleanliness, and is pollution-free. In view of this situation, great effort has been made to reduce NO_x. Nakatsuji et al. achieved the regeneration of Rh-based catalysts with H_2 produced during the strong combustion phase (Nakatsuji and Komppa, 2002). Otherwise, Crocker reported that ceria has a good capacity to store oxygen, which could improve the storage capacity of NSR catalysts and thus reduce NO_x easily (Ji et al., 2008).

The strategies to improve the catalytic activity of noble metals have been widely investigated (Jiang et al., 2020; Kuai et al., 2020). The unique chemical structure always played an important role in influencing reactions. The recent examples include the following: (1) a Pt_1/FeO_x single-atom catalyst showed a higher catalytic performance, which greatly improved the utilization of a single atom (Qiao et al., 2011); (2) single Pt atoms were fixed on the surface of defective TiO_2 in which way the increased concentration of oxygen vacancy enhanced photocatalytic performance (Chen et al., 2020); and (3) the *in-situ* formation of a metal bond M-Co (M = Pt, Rh, and Pd) structure during the reaction promoted the reduction of NO (Wang et al., 2013; Nguyen et al., 2016). Based on the above research, the strategy of how to construct a new structure with high performance was of great significance to the development of highly efficient catalysts.

In our work, we proposed and validated a new structure of Pt-O-Ce^{3+} to remove NO_x effectively. The triggering mechanism was confirmed by replacing Ce atoms with Pt atoms of low valence states, described as PtCe(N) catalyst whose Pt atoms were derived from platinum nitrate solution. Then the introduction of such Pt atoms would cause a redistribution of charge on the surface of CeO_2, resulting in the increase of oxygen vacancies and Ce^{3+} sites. When served as a catalyst for reducing NO_x, the PtCe(N) catalyst exhibited a superior low-temperature capability of removal of NO_x. The results would help to provide a deep understanding of the relationship between structure and efficiency, which was regarded as a valuable strategy for the design and synthesis of new de-NO_x catalysts.

EXPERIMENTAL

Catalyst Preparation

The ceria nanorods were synthesized according to the hydrothermal method (Fu et al., 2019). In total, 1.74 g $Ce(NO_3)_3{\cdot}6H_2O$ was added into 5 ml deionized water with vigorous stirring for 30 min, and 19.2 g NaOH was dissolved in 65 ml deionized water. After $Ce(NO_3)_3{\cdot}6H_2O$ and NaOH were fully dissolved in water, two solutions were mixed up and stirred for another 30 min. Then, the mixed solution was transferred to a Teflon bottle and further tightly sealed in a stainless-steel autoclave. The thermal procedure of catalysts was performed to heat at 100° for 24 h in an oven. When cooling to room temperature, the solution was washed with deionized water and anhydrous ethanol several times. The solid powder was obtained by drying in air at 80° overnight, and ceria nanorods were obtained by calcining in air at 500° for 4 h with the rate of $5°{\cdot}min^{-1}$.

Ceria-supported different platinum precursors were synthesized by the wet mpregnation method (Spezzati et al., 2017; DeRita et al., 2019). In total, 0.5 g CeO_2 was dispersed in 40 ml deionized water, and 2.5 ml (1 $mg{\cdot}ml^{-1}$) platinum nitrate [$Pt(NO_3)_2$] solution was dropped into the above suspension under vigorously stirring at 70° for 4 h. The precipitate was washed with deionized water and selected via centrifugal mode. After drying overnight at 80°, the sample was calcined at 300° for 4 h in muffle oven. Then the catalysts were obtained, which were described as PtCe(N). Uniformly, the preparation method of PtCe(C) catalysts was the same as that of PtCe(N) catalysts, except for replacing the platinum nitrate with chloroplatinic acid (H_2PtCl_6). By means of heat treatment and calcination, $[PtCl_6]^{2-}$ species were dechlorinated and little Cl ion was detected (Zhang et al., 2019; Ye et al., 2020). Meanwhile, the Pt content was the same on the PtCe(N) and PtCe(C) catalyst (0.204% vs. 0.209%), as determined by ICP-MS. Noteworthily, the Pt atoms from platinum nitrate solution and chloroplatinic acid solution were divalent [Pt(II)] and tetravalent [Pt(IV)], respectively.

Catalyst Characterizations

For the structural analyses of the catalyst, transmission electron microscopy (TEM) and field-emission high-resolution transmission electron microscopy (HRTEM) measurements were carried out on a JEOL JEM 2100F microscope operating at an accelerating voltage of 200 kV. The powder X-ray diffraction (XRD) was carried out on a Rigaku D/MAX 2500v/PC X-ray diffractometer with Cu-Ka radiation (λ = 0.15418 nm). The nitrogen adsorption–desorption isotherms were measured using a Quantachrome Autosorb IQ instrument at −196°C. The specific surface area was calculated by the Brunauer-Emmett-Teller (BET) equation and the pore size distribution was determined using a cylindrical pore model (BJH method). The X-ray photoelectron spectroscopy (XPS) analysis was recorded on a surface analysis system (Thermal ESCALAB 250 spectrometer) equipped with Al Ka monochromatized radiation. The C 1s peak at 284.6 eV was used as a reference, and these kinds of peaks were calibrated by C 1s peak standardized at 284.6 eV. Raman spectra were carried out on a TEO SR-500I-A Raman spectrometer with the excitation laser wavelength of 532 nm. Detailed information on the surface defects was obtained using electron paramagnetic resonance (EPR) performed using an electron paramagnetic resonance spectrometer (Bruker E500) at room temperature. Hydrogen temperature-programmed reduction (H_2-TPR) was carried out on a Micromerities Autochem 2920II instrument in order to obtain the reducibility of the catalysts. Firstly, the catalyst (100 mg) was pretreated in Ar (25 $ml{\cdot}min^{-1}$) at 100°C for 1 h, and then cooled to ambient temperature. After then, the sample was heated in 10% H_2/Ar from room temperature to 1000°C at a heating rate of $10°C{\cdot}min^{-1}$.

Catalytic Tests

The catalytic activity tests were performed at atmospheric with a fixed-bed continuous flow quartz microreactor (inner diameter

= 10 mm). In total, 0.1 g catalyst (40∼60 mesh) was used to reduce NO_x with H_2. The flow rate of the reaction gas was 100 ml·min^{-1} accompanied with 1000 ppm NO, 4000 ppm H_2 and balanced with argon, and the corresponding gas hourly space velocity (GHSV) was about 60,000 ml·g^{-1}·h^{-1}. The component and concentration of outlet gas can be obtained by KM-940 flue gas analyzer (Kane International Limited, UK). The NO_x conversion rate was calculated by the following equations:

$$NO_x \text{ conversion } (\%) = 100\% \times \frac{[NO_x]_{in} - [NO_x]_{out}}{[NO_x]_{in}}$$

The $[NO_x]_{in}$ and $[NO_x]_{out}$ noted the inlet and outlet concentration at a steady state and separately ($[NO_x] = [NO] + [NO_2]$).

RESULTS AND DISCUSSION

Catalytic Activity

Figure 1A showed the conversion of NO_x at different temperatures (50–200°) on CeO_2 based catalysts with different platinum precursors. Across the whole temperature range, CeO_2 catalysts had almost no activity for NO_x removal. It proved Pt atoms were the active center in the catalytic reaction directly. Lower than 75°, all catalysts showed poor activity. Compared with PtCe(C) catalysts with rising temperatures, PtCe(N) catalysts exhibited much better activity. Especially the NO_x conversion of PtCe(N) catalysts reached 90% at 125°, which showed ∼70% efficiency higher than PtCe(C) catalysts. When 100% NO_x conversion was achieved over PtCe(N) catalysts from 150 to 200°, the activity of PtCe(C) was still lower though the activity curve was going up. These results showed a platinum nitrate precursor supported on CeO_2 supports could greatly promote the performance of catalysts at a lower temperature. Moreover, the thermal stability of catalysts was measured to verify materials' availability. The temperature at 175° was chosen for the test because of its good activity (60 vs. 100%) over both PtCe(C) and PtCe(N) catalysts. Specifically, they behaved perfect thermal stability within constant reaction gas after 48 h (**Figure 1B**). What's more, activation energy could be used to express the minimum energy required for a reaction to occur, and the magnitude of activation energy could reflect the difficulty of the chemical reaction. As shown in **Figure 1C**, the apparent energy of reaction catalyzed by PtCe(N) (Ea = 28.5 kJ/mol) was smaller compared with PtCe(C) (Ea = 44.5 kJ/mol) based on Arrhenius plots. It was recognized that the lower the activation energy the better the reaction. The results were consistent with the catalytic activity curve (**Figure 1A**). Superior catalytic performance of PtCe(N) catalysts implied stronger interaction existed between Pt atoms and CeO_2 supports in the reaction, which might due to the introduction of different platinum precursors. So, various characterizations were carried out to investigate the relationship between structure and catalytic activities (Macino et al., 2019).

Morphology and Structure

To explore reasons for the difference in catalytic performance, the morphology and microstructure were investigated in detail by high-resolution transmission electron microscope (HRTEM) and energy-dispersive X-ray spectroscopy (EDXS) mappings (**Figure 2**). The images perfectly showed the CeO_2 in the shape of nanorods (**Figures 2A,B**). The lattice fringe was about 3.1 Å, assigned to the interplanar distance of (111) plane of CeO_2. Otherwise, EDXS mapping revealed the uniform dispersion of Ce and O elements on CeO_2 nanorods (**Figure 2C**). The Pt atoms were easily loaded at the surface of CeO_2 nanorods. The results showed that series of CeO_2 based catalysts showed the same phase and similar morphology (**Figures 2D–I**), indicating that the difference in catalytic performance was not directly related to the micromorphology. Moreover, as shown in **Figures 2F,I**, EDXS mappings of PtCe(C) and PtCe(N) catalysts showed that Pt atoms were successfully dispersed in all of the CeO_2 catalysts (Li et al., 2019). And the content of Cl ion in PtCe(C) was also detected by the TEM-EDXS (**Supplementary Figure 1**; **Supplementary Table 1**). The results showed that there was little Cl ion in the sample and far less than the Pt content.

The effect of Pt atoms incorporation on the structure of CeO_2 supports was first verified. The X-ray diffraction (XRD) patterns of catalysts before and after the introduction of Pt atoms were shown in **Figure 3A** and **Supplementary Figure 2**. Each sample exhibited a CeO_2 spinel phase (PDF NO. 34-0394). It could be seen that CeO_2 nanorods had perfect crystallinity with mainly (111) facet exposed, which was extremely consistent with the lattice fringe of 3.1 Å from HRTEM images. In addition, the characteristic peaks at 33.1°, 47.5°, 56.3°, 59.1°, 69.4°, 76.7°, 79.1°, and 88.4° corresponding to the (200), (220), (311), (222), (400), (331), (420), and (422) planes of the CeO_2 spinel phase, respectively. Compared with CeO_2 catalysts, the crystalline of PtCe(C) and PtCe(N) catalysts tended to increase after the introduction of Pt atoms. The results showed Pt atoms might play an important role to stabilize the crystalline phase of CeO_2. In addition, there were no significant changes in the position of characteristic peaks, and no diffraction peaks ascribed to Pt species were detected on catalysts, indicating that Pt species were highly dispersed on catalysts or their grain size were below the detection limit of XRD (Xu et al., 2018, 2019).

The N_2 adsorption-desorption isotherms on CeO_2, PtCe(C), and PtCe(N) catalysts were carried out to explore the specific surface and pore structure after the addition of Pt atoms (**Figures 3B,C**). All catalysts followed the mesoporous structure curve, and the relevant data were listed in **Table 1**. The BET-specific surface areas of PtCe(C) (81.16 m^2·g^{-1}) and PtCe(N) (87.93 m^2·g^{-1}) catalysts were similar to that of CeO_2 support (86.35 m^2·g^{-1}). But both pore volume and average pore diameter on catalysts loaded with platinum showed a decrease obviously, which might due to blockages caused by Pt atoms in the pores. It was known that Pt atoms are larger in diameter than Ce atoms. It was a possible reason to cause changes of specific surface and pore structure by replacing Ce atoms with Pt atoms.

Surface Element Composition and Status

X-ray photoelectron spectroscopy (XPS) technique was performed to investigate the surface components and valence

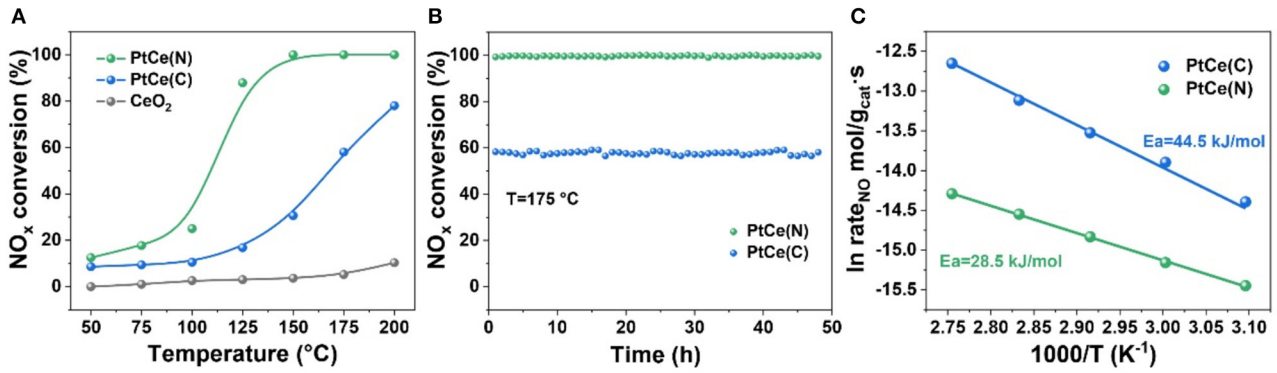

FIGURE 1 | (A) NO_x conversion as a function of temperature over CeO_2, PtCe(C), and PtCe(N) catalysts. **(B)** The thermal stability of PtCe(C) and PtCe(N) catalysts. Reaction conditions: 1000 ppm NO, 4000 ppm H_2 balanced with Ar, 60 000 ml·g^{-1}·h^{-1}. **(C)** The arrhenius plot of reaction rate for the PtCe(C) and PtCe(N) catalysts.

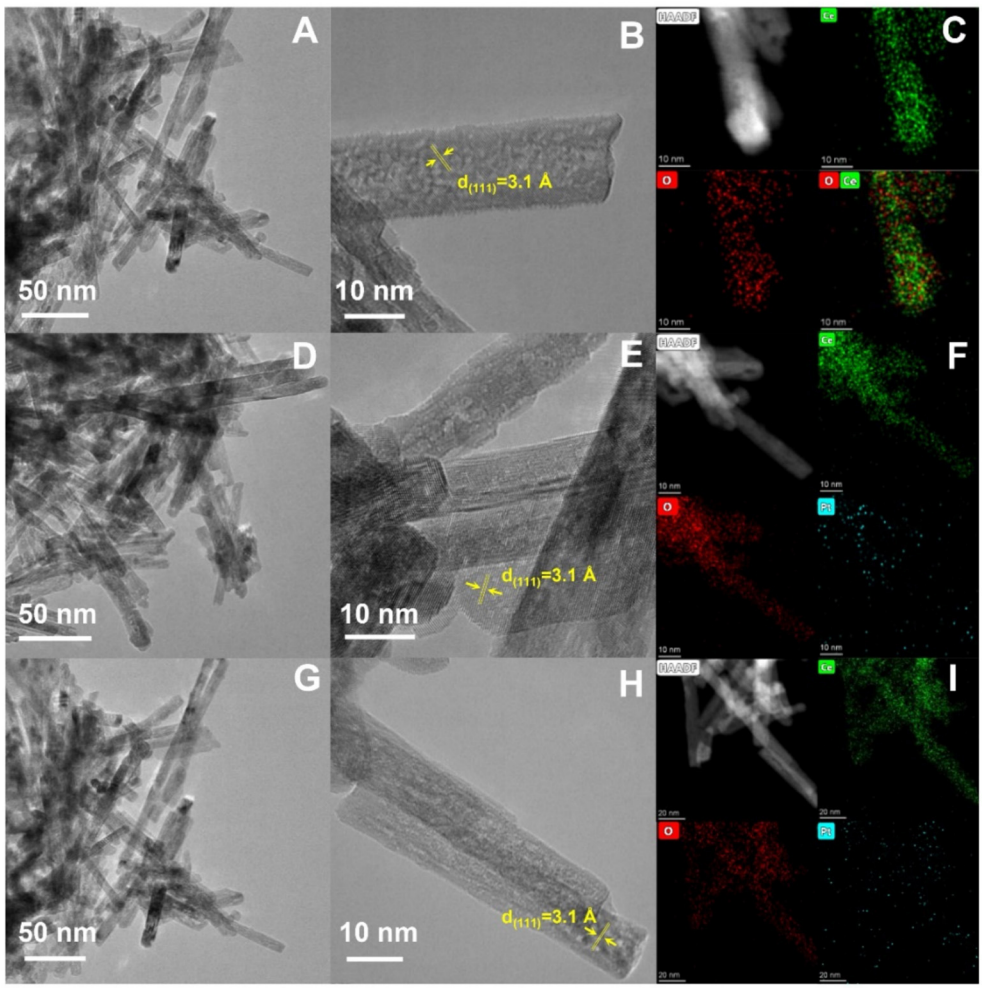

FIGURE 2 | TEM and HRTEM images and corresponding EDXS mappings of CeO_2 **(A–C)**, PtCe(C) **(D–F)**, and PtCe(N) **(G–I)** catalysts.

states of the elements on catalysts (Xu et al., 2020). The normalized band areas of Pt 4f, Ce 3d, and O 1s XPS spectra are shown in **Figure 4**, and the surface atomic concentrations are listed in **Table 2**. **Figure 4A** exhibits the Pt 4f XPS spectrum with two characteristic peaks at 76.3 and 73.0 eV on PtCe(C) catalysts, which showed that $Pt^{\delta+}$ with a high oxidation state

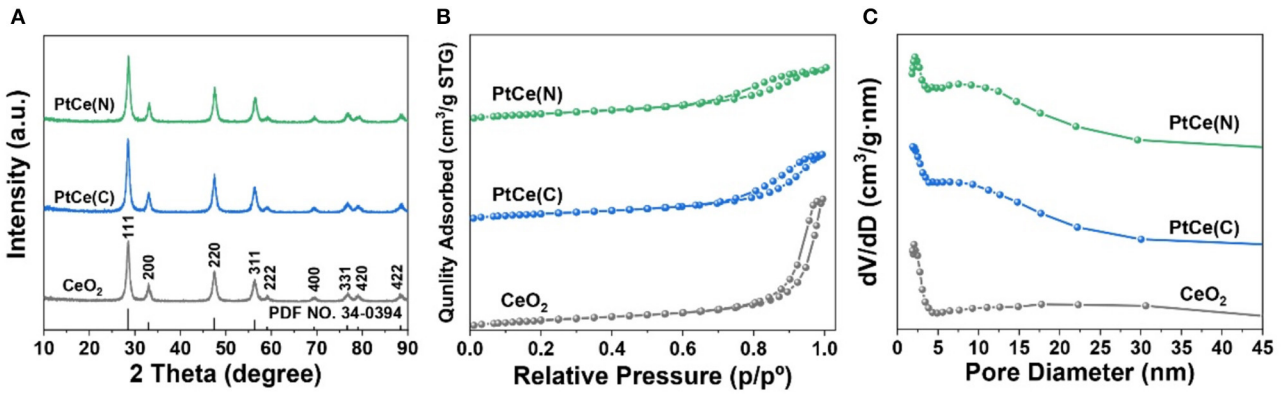

FIGURE 3 | The XRD patterns **(A)**, nitrogen adsorption-desorption isotherm **(B)** and pore size distribution **(C)** of CeO_2, PtCe(C), and PtCe(N) catalysts.

TABLE 1 | Summary of textual parameters of the catalysts.

Catalysts	Specific area (m^2/g)	Pore volume (cm^3/g)	Average pore diameter (nm)
CeO_2	86.35	0.46	18.97
PtCe(C)	81.16	0.17	7.47
PtCe(N)	87.93	0.19	8.20

(δ was 2∼4) was the primary species (Mukri et al., 2013). Different from PtCe(C) catalysts, four peaks of Pt 4f were found at ∼75.9, 74.0, 71.9, and 70.6 eV in which the binding energy at 70.6 eV agreed with that of Pt metal and the binding energy at 71.9 eV was about 0.8 eV lower than Pt(II) oxide (Pereira-Hernandez et al., 2019). The results indicated that the Pt atoms over PtCe(N) catalysts tended to a lower valence state between Pt^0 and Pt^{2+}. The binding energy of Pt 4f over PtCe(C) and PtCe(N) catalysts was lower than those of Pt(IV) and Pt(II), respectively, suggesting that there was a strong electronic interaction between Pt atoms and CeO_2. Another different phenomenon pointed to the O 1s XPS spectrum (**Figure 4B**). Referring to relevant literature, the peaks at low binding energy from 529.3 to 529.7 eV were ascribed to the lattice oxygen (O_{latt}), while the peak at high binding energy from 530.9 to 531.1 eV was assigned to the surface-adsorbed oxygen (O_{ads}) (Han et al., 2019a). It was noticed the ratio of $O_{ads}/(O_{ads} + O_{latt})$ increased to 27.1% on PtCe(N) catalysts compared to 25.6% for CeO_2 supports and 25.5% for PtCe(C) catalysts. The only variable in our system was the introduction of different platinum precursors, suggesting Pt (II) atoms doping could greatly create extra oxygen vacancies. As shown in **Figure 4C**, the XPS peak of Ce 3d was fitted into 10 overlapping peaks on all catalysts. The peaks assigned to u′ and v′ were the main representatives of the $3d^{10}4f^1$ electronic state of Ce^{3+}, while u_o, u, u″, u‴, v_o, v, v″, and v‴ peaks represented the $3d^{10}4f^0$ electronic state of Ce^{4+} (Wang M. et al., 2019). Results of the Ce^{3+} content $[Ce^{3+}/(Ce^{3+} + Ce^{4+})]$ were shown in **Table 2**. There were a larger Ce^{3+} percentage (13.2%) on PtCe(N) catalysts. The Ce^{3+} rations were higher than those of the PtCe(C) catalysts (10.1%) and CeO_2 supports (10.4%). It was known that the formation of Ce^{3+} was directly related to the presence of oxygen vacancies. Compared with PtCe(C) catalysts, a series of variations proved the substitution of Ce (IV) atoms by Pt (II) atoms on PtCe(N) catalysts generated more oxygen vacancies and Ce^{3+} sites, forming a structure of Pt-O-Ce^{3+}. The unique Pt-O-Ce^{3+} structures might enhance the catalytic activity. Otherwise, the used catalysts were also tested with XPS measurement (**Figures 4D–I**), and no significant changes were found among Pt 4f, Ce 3d, and O 1s XPS spectra, realizing all catalysts were stable before and after the reaction (Wang R. et al., 2019).

Identification of Pt-O-Ce^{3+} Structure

The molecular structure and composition of catalysts were further investigated by Raman spectroscopy. As shown in **Figure 5A**, CeO_2 was the crystal possessing the fluorite structure with a space group, and there was only one triply degenerate Raman-active optical phonon with frequency at about 464 cm^{-1}. Except for the characteristic peak at 464 cm^{-1}, there were two other peaks at 598 and 970 cm^{-1} that appeared after the introduction of Pt atoms. For the Raman spectrum of catalysts at 598 cm^{-1}, it represented the Frenkel-type oxygen vacancies created by the relocation of oxygen anions from tetrahedral sites to octahedral sites, which was caused by the defect sites in the crystal lattice (Guo et al., 2018; Fan et al., 2019). Compared with CeO_2 catalysts, the signal at 598 cm^{-1} was significantly enhanced on the PtCe(C) and PtCe(N) catalysts. And the strongest signals were found over PtCe(N) catalysts, indicating more oxygen vacancies were formed on the surface of CeO_2 after introducing Pt atoms. It was consistent with XPS results. Moreover, the peak at 970 cm^{-1} assigned to the asymmetric structure of Pt-O-Ce was obviously found on PtCe(N) catalysts (Huang et al., 2014; Wang et al., 2015). The formation of the new structure was recognized as the most intuitive evidence that Pt atoms replaced Ce atoms on the surface of CeO_2. As a consequence, the charge population around substitution sites was changed after the Pt (II) atoms replaced Ce (IV) atoms. Combined

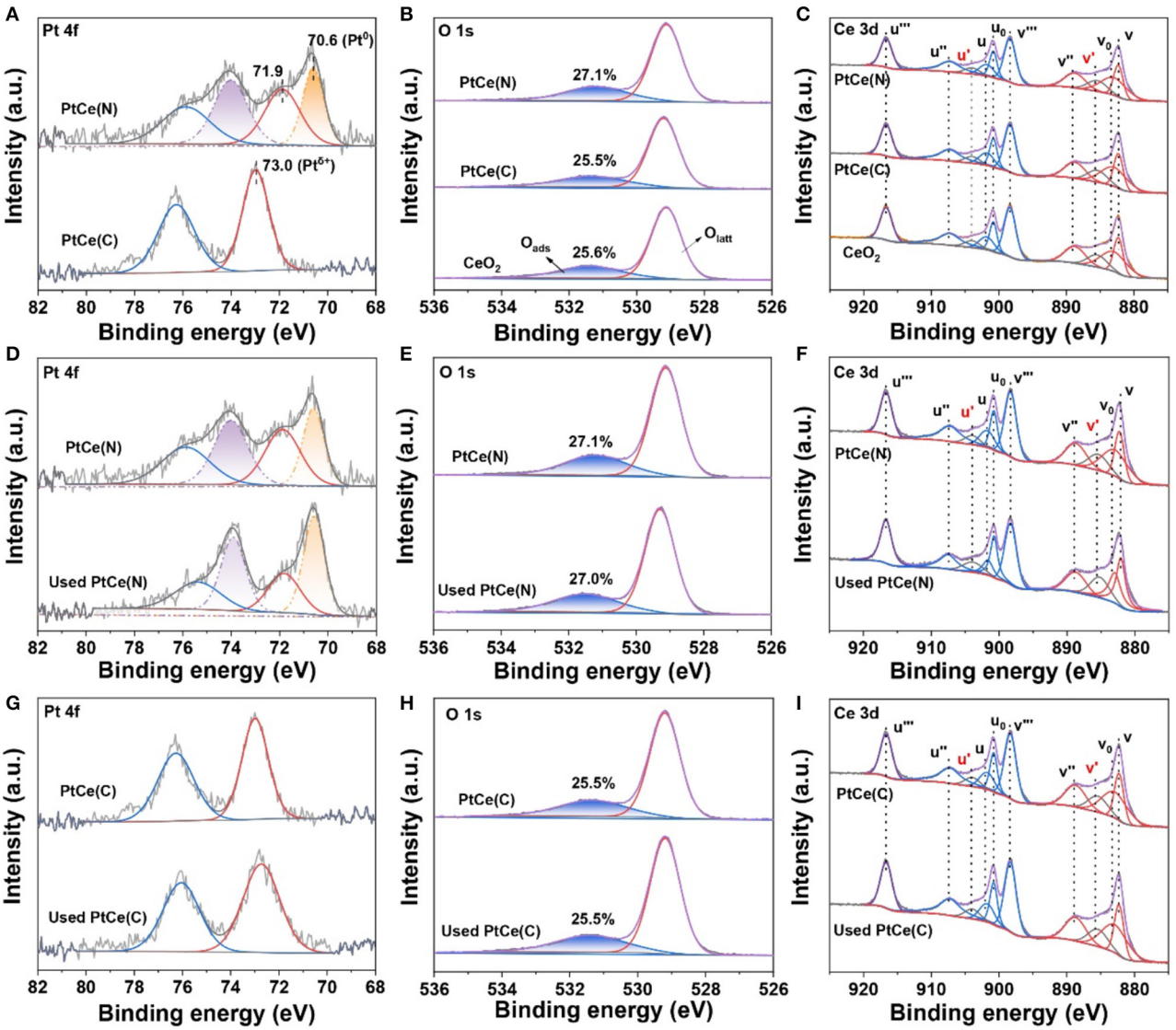

FIGURE 4 | XPS spectra for CeO_2, PtCe(N), and PtCe(C) catalysts of Pt 4f, Ti 2p, and O 1s **(A–C)**. XPS spectra for PtCe(N) and used PtCe(N) catalysts of Pt 4f, Ti 2p, and O1s **(D–F)**. XPS spectra for PtCe(C) and used PtCe(C) catalysts of Pt 4f, Ti 2p, and O1s **(G–I)**.

with XPS results, oxygen vacancies were used to balance the reduced valence, accompanied by the increase in Ce^{3+} content. On the contrary, it was found that a weak signal of Pt-O-Ce structure occurred on PtCe(C) catalysts from the Raman spectrum. Despite the existence of the substitution phenomenon, the introduction of Pt (IV) atoms didn't cause the increase of oxygen vacancies. The difference might directly relate to the activity of the catalytic reaction.

The electron paramagnetic resonance (EPR) measurement was further performed to get more information about oxygen vacancies on different catalysts. As shown in **Figure 5B**, CeO_2 had a signal at $g = 2.001$ at room temperature, which was assigned to the existence of oxygen vacancies (Pan et al., 2013; Li et al., 2018). Similarly, the PtCe(C) catalysts showed the same signal strength as CeO_2, indicting constant density of oxygen vacancies after loading with Pt (IV) atoms. It was noted that the EPR signals of PtCe(N) catalysts were remarkably strong at $g = 2.001$, which was consistent with the results of XPS and

TABLE 2 | The valence ratios of surface elements.

Catalysts	O 1s		Ce 3d	
	$O_{ads}/(O_{ads} + O_{latt})$	O_{ads}/O_{latt}	$Ce^{3+}/(Ce^{3+} + Ce^{4+})$	Ce^{3+}/Ce^{4+}
CeO_2	25.6%	0.34	10.4%	0.12
PtCe(C)	25.5%	0.34	10.1%	0.11
PtCe(N)	27.1%	0.37	13.2%	0.15
Used PtCe(C)	25.5%	0.34	10.5%	0.12
Used PtCe(N)	27.0%	0.37	13.0%	0.15

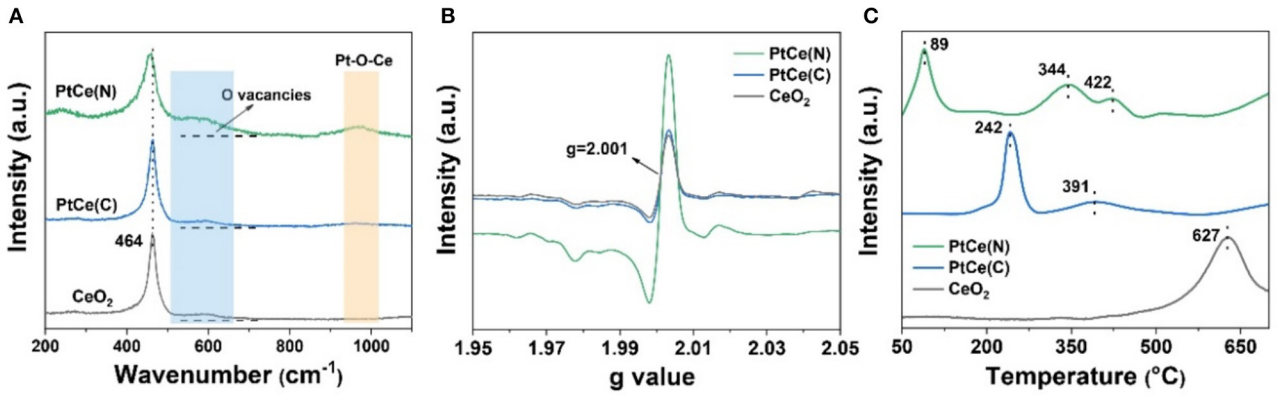

FIGURE 5 | The Raman spectra **(A)**, EPR spectra **(B),** and H_2-TPR profiles **(C)** of CeO_2, PtCe(C), and PtCe(N) catalysts.

Raman. On the basis of the experiment, the defect was attributed to the presence of oxygen vacancies in the lattice, by means of replacing Ce atoms with Pt (II) atoms. As a consequence, the structure of Pt-O-Ce^{3+} was beneficial to promote the catalytic reaction.

The redox ability of catalysts was confirmed with hydrogen temperature-programmed reduction (H_2-TPR) (**Figure 5C**). For CeO_2 supports, there was only one main peak that appeared at 627 cm^{-1}, which was ascribed to the reduction of bulk oxygen of CeO_2 (bulk Ce^{4+} to Ce^{3+}) (Yan et al., 2020). After Pt atoms doped, the peak shifted to a lower temperature range of 340–430° on PtCe(C) (344 and 422°) and PtCe(N) (391°) catalysts, indicating the improvement of redox ability on Pt-based catalysts. Otherwise, the peak loaded at 89° was found on PtCe(N) catalysts, which was attributed to the PtO_x species strongly interacting with CeO_2 supports. Similarly, a weaker interaction between PtO_x species and CeO_2 supports was discovered on PtCe(C) catalysts from the peak of 242° (Wang et al., 2015; Duan et al., 2017). The results could well explain the Pt (II) atoms greatly enhanced the interaction between metal and support due to the formation of Pt-O-Ce^{3+} structures.

CONCLUSIONS

In summary, CeO_2-based catalysts loading with different Pt precursors were successfully prepared for the reduction of NO with H_2. PtCe(N) exhibited excellent de-NO_x performance (>80%) over a wide operating temperature (125–200°) as well as excellent thermal stability. According to the results of XPS, Raman, and EPR, Pt (II) atoms of platinum nitrate could replace Ce (IV) atoms on the surface of CeO_2 nanorods during the synthetic process, and thus the local charge environment would change accordingly. This might result in an increment of oxygen vacancies and Ce^{3+} sites, which could balance the negative charge and enhance the electronic metal-support interactions. Furthermore, we proposed a triggering mechanism to form unique structures, and we confirmed the Pt-O-Ce^{3+} ensemble was the base unit in the high-performance PtCe(N) catalyst. In addition, compared to PtCe(N) catalysts, no obvious changes about surface components and valence states were found on PtCe(C) catalysts, and this was accompanied by a 40% drop in NO_x conversion. This work provided a strategy to develop high-efficiency de-NO_x catalysts.

DATA AVAILABILITY STATEMENT

The original contributions presented in the study are included in the article/**Supplementary Material**, further inquiries can be directed to the corresponding author.

AUTHOR CONTRIBUTIONS

GL, ZH, and SZ designed the research. GL and ZH conducted the fabrication and sample characterizations. XM and NM helped with sample fabrication and processing. GL, ZH, and SZ wrote the manuscript. HZ and YL helped improve the manuscript. All authors listed have made a substantial, direct and intellectual contribution to the work, and approved it for publication and contributed to the discussion of the manuscript.

FUNDING

This work was supported by the National Natural Science Foundation of China (grant Nos. 22076082 and 21874099), the Tianjin Commission of Science and Technology as key technologies R&D projects (grant Nos. 18YFZCSF00730, 18YFZCSF00770, 18ZXSZSF00230, 19YFZCSF00740, and 20YFZCSN01070).

SUPPLEMENTARY MATERIAL

The Supplementary Material for this article can be found online at: https://www.frontiersin.org/articles/10.3389/fenvc.2021.672844/full#supplementary-material

REFERENCES

Abdulhamid, H., Fridell, E., and Skoglundh, M. (2003). Influence of the type of reducing agent (H_2, CO, C_3H_6 and C_3H_8) on the reduction of stored NO_x in a $Pt/BaO/Al_2O_3$ model catalyst. *Top. Catal.* 30, 1–4. doi: 10.1023/B:TOCA.0000029745.87107.b8

Anenberg, S. C., Miller, J., Minjares, R., Du, L., Henze, D. K., and Lacey, F., et al. (2017). Impacts and mitigation of excess diesel-related NO_x emissions in 11 major vehicle markets. *Nature* 545, 467–471. doi: 10.1038/nature22086

Chen, Y., Ji, S., Sun, W., Lei, Y., Wang, Q., and Li, A., et al. (2020). Engineering the atomic interface with single platinum atoms for enhanced photocatalytic hydrogen production. *Angew. Chem. Int. Ed. Engl.* 59, 1295–1301. doi: 10.1002/anie.201912439

DeRita, L., Resasco, J., Dai, S., Boubnov, A., Thang, H. V., and Hoffman, A. S., et al. (2019). Structural evolution of atomically dispersed Pt catalysts dictates reactivity. *Nat. Mater.* 18, 746–751. doi: 10.1038/s41563-019-0349-9

Duan, Z., Chi, K., Liu, J., Shi, J., Zhao, Z., and Wei, Y., et al. (2017). The catalytic performances and reaction mechanism of nanoparticle Cd/Ce-Ti oxide catalysts for NH_3-SCR reaction. *RSC Adv.* 7, 50127–50134. doi: 10.1039/C7RA06931F

Fan, Z., Wang, Z., Shi, J., Gao, C., Gao, G., and Wang, B., et al. (2019). Charge-redistribution-induced new active sites on (001) facets of α-Mn_2O_3 for significantly enhanced selective catalytic reduction of NO by NH_3. *J. Catal.* 370, 30–37. doi: 10.1016/j.jcat.2018.12.001

Fu, X., Guo, L., Wang, W., Ma, C., Jia, C., and Wu, K., et al. (2019). Direct identification of active surface species for the water-gas shift reaction on a gold-ceria catalyst. *J. Am. Chem. Soc.* 141, 4613–4623. doi: 10.1021/jacs.8b09306

Guo, Y., Mei, S., Yuan, K., Wang, D., Liu, H., and Yan, C., et al. (2018). Low-temperature CO_2 methanation over CeO_2-supported Ru single atoms, nanoclusters, and nanoparticles competitively tuned by strong metal-support interactions and H-spillover effect. *ACS Catal.* 8, 6203–6215. doi: 10.1021/acscatal.7b04469

Han, L., Gao, M., Feng, C., Shi, L., and Zhang, D. (2019a). Fe_2O_3-CeO_2@Al_2O_3 nanoarrays on Al-mesh as SO_2-tolerant monolith catalysts for NO_x reduction by NH_3. *Environ. Sci. Technol.* 53, 5946–5956. doi: 10.1021/acs.est.9b01217

Han, L., Gao, M., Hasegawa, J. Y., Li, S., Shen, Y., and Li, H., et al. (2019b). SO_2-tolerant selective catalytic reduction of NO_x over Meso-TiO_2@Fe_2O_3@Al_2O_3 metal-based monolith catalysts. *Environ. Sci. Technol.* 53, 6462–6473. doi: 10.1021/acs.est.9b00435

Huang, H., Dai, Q., and Wang, X. (2014). Morphology effect of Ru/CeO_2 catalysts for the catalytic combustion of chlorobenzene. *Appl. Catal. B* 158–159, 96–105. doi: 10.1016/j.apcatb.2014.01.062

Ji, Y., Choi, J. S., Toops, T. J., Crocker, M., and Naseri, M. (2008). Influence of ceria on the NO_x storage/reduction behavior of lean NO_x trap catalysts. *Catal. Today* 136, 146–155. doi: 10.1016/j.cattod.2007.11.059

Jiang, L., Liu, K., Hung, S., Zhou, L., Qin, R., and Zhang, Q., et al. (2020). Facet engineering accelerates spillover hydrogenation on highly diluted metal nanocatalysts. *Nat. Nanotechnol.* 15, 848–853. doi: 10.1038/s41565-020-0746-x

Jozsa, P., Jobson, E., and Larsson, M. (2004). Reduction of NO_x stored at low temperatures on a NO_x adsorbing catalyst. *Top. Catal.* 30, 1–4. doi: 10.1023/B:TOCA.0000029837.68739.55

Kuai, L., Chen, Z., Liu, S., Kan, E., Yu, N., and Ren, Y., et al. (2020). Titania supported synergistic palladium single atoms and nanoparticles for room temperature ketone and aldehydes hydrogenation. *Nat. Commun.* 11:48. doi: 10.1038/s41467-019-13941-5

Li, J., Guan, Q., Wu, H., Liu, W., Lin, Y., and Sun, Z., et al. (2019). Highly active and stable metal single-atom catalysts achieved by strong electronic metal-support interactions. *J. Am. Chem. Soc.* 141, 14515–14519. doi: 10.1021/jacs.9b06482

Li, J., Zhou, H., Zhuo, H., Wei, Z., Zhuang, G., and Zhong, X., et al. (2018). Oxygen vacancies on TiO_2 promoted the activity and stability of supported Pd nanoparticles for the oxygen reduction reaction. *J. Mater. Chem. A* 6, 2264–2272. doi: 10.1039/C7TA09831F

Macino, M., Barnes, A. J., Althahban, S. M., Qu, R., Gibson, E. K., and Morgan, D. J., et al. (2019). Tuning of catalytic sites in Pt/TiO_2 catalysts for the chemoselective hydrogenation of 3-nitrostyrene. *Nat. Catal.* 2, 873–881. doi: 10.1038/s41929-019-0334-3

Mukri, B., Waghmare, U., and Hegde, M. (2013). Platinum ion-doped TiO_2: high catalytic activity of Pt^{2+} with oxide ion vacancy in $Ti^{4+}_{1-x}Pt^{2+}_xO_{2-x}$ compared to Pt^{4+} without oxide ion vacancy in $Ti^{4+}_{1-x}Pt^{4+}_xO_2$. *Chem. Mater.* 25, 3822–3833. doi: 10.1021/cm4015404

Nakatsuji, T., and Komppa, V. (2002). A catalytic NO_x reduction system using periodic steps, lean, and rich operations. *Catal. Today* 75, 407–412. doi: 10.1016/S0920-5861(02)00090-1

Nguyen, L., Zhang, S., Wang, L., Li, Y., Yoshida, H., and Patlolla, A., et al. (2016). Reduction of nitric oxide with hydrogen on catalysts of singly dispersed bimetallic sites Pt_1Co_m and Pd_1Co_n. *ACS Catal.* 6, 840–850. doi: 10.1021/acscatal.5b00842

Oberschelp, C., Pfister, S., Raptis, C. E., and Hellweg, S. (2019). Global emission hotspots of coal power generation. *Nat. Sustain.* 2, 113–121. doi: 10.1038/s41893-019-0221-6

Pan, X., Yang, M., Fu, X., Zhang, N., and Xu, Y. (2013). Defective TiO_2 with oxygen vacancies: synthesis, properties, and photocatalytic applications. *Nanoscale* 5, 3601–3614. doi: 10.1039/c3nr00476g

Pereira-Hernandez, X. I., DeLaRiva, A., Muravev, V., Kunwar, D., Xiong, H., and Sudduth, B., et al. (2019). Tuning Pt-CeO_2 interactions by high-temperature vapor-phase synthesis for improved reducibility of lattice oxygen. *Nat. Commun.* 10:1358. doi: 10.1038/s41467-019-09308-5

Pronk, A., Coble, J., and Stewart, P. A. (2009). Occupational exposure to diesel engine exhaust: a literature review. *J. Expo. Sci. Environ. Epidemiol.* 19, 443–457. doi: 10.1038/jes.2009.21

Qiao, B., Wang, A., Yang, X., Allard, L. F., Jiang, Z., and Cui, Y., et al. (2011). Single-atom catalysis of CO oxidation using Pt_1/FeO_x. *Nat. Chem.* 3, 634–641. doi: 10.1038/nchem.1095

Spezzati, G., Su, Y., Hofmann, J. P., Benavidez, A. D., DeLaRiva, A. T., and McCabe, J., et al. (2017). Atomically dispersed Pd-O species on CeO_2(111) as highly active sites for low-temperature CO oxidation. *ACS Catal.* 7, 6887–6891. doi: 10.1021/acscatal.7b02001

Wang, F., Li, C., Zhang, X., Wei, M., Evans, D., and Duan, X. (2015). Catalytic behavior of supported Ru nanoparticles on the {100}, {110}, and {111} facet of CeO_2. *J. Catal.* 329, 177–186. doi: 10.1016/j.jcat.2015.05.014

Wang, L., Zhang, S., Zhu, Y., Patlolla, A., Shan, J., and Yoshida, H., et al. (2013). Catalysis and in situ studies of Rh_1/Co_3O_4 nanorods in reduction of NO with H_2. *ACS Catal.* 3, 1011–1019. doi: 10.1021/cs300816u

Wang, M., Shen, M., Jin, X., Tian, J., Li, M., and Zhou, Y., et al. (2019). Oxygen vacancy generation and stabilization in CeO_{2-x} by Cu introduction with improved CO_2 photocatalytic reduction activity. *ACS Catal.* 9, 4573–4581. doi: 10.1021/acscatal.8b03975

Wang, R., Hao, Z., Li, Y., Liu, G., Zhang, H., and Wang, H., et al. (2019). Relationship between structure and performance of a novel highly dispersed MnO_x on Co-Al layered double oxide for low temperature NH_3-SCR. *Appl. Catal. B* 258:117983. doi: 10.1016/j.apcatb.2019.117983

Xu, H., Liu, J., Zhang, Z., Liu, S., Lin, Q., and Wang, Y., et al. (2019). Design and synthesis of highly-dispersed WO_3 catalyst with highly effective NH_3-SCR activity for NO_x abatement. *ACS Catal.* 9, 11557–11562. doi: 10.1021/acscatal.9b03503

Xu, H., Liu, S., Wang, Y., Lin, Q., Lin, C., and Lan, L., et al. (2018). Promotional effect of Al_2O_3 on WO_3/CeO_2-ZrO_2 monolithic catalyst for selective catalytic reduction of nitrogen oxides with ammonia after hydrothermal aging treatment. *Appl. Surf. Sci.* 427, 656–669. doi: 10.1016/j.apsusc.2017.08.166

Xu, Q., Fang, Z., Chen, Y., Guo, Y., Guo, Y., and Wang, L., et al. (2020). Titania-samarium-manganese composite oxide for the low-temperature selective catalytic reduction of NO with NH_3. *Environ. Sci. Technol.* 54, 2530–2538. doi: 10.1021/acs.est.9b06701

Yan, L., Wang, F., Wang, P., Impeng, S., Liu, X., and Han, L., et al. (2020). Unraveling the unexpected offset effects of Cd and SO_2 deactivation over CeO_2-WO_3/TiO_2 catalysts for NO_x reduction. *Environ. Sci. Technol.* 54, 7697–7705. doi: 10.1021/acs.est.0c01749

Ye, X., Yang, C., Pan, X., Ma, J., Zhang, Y., and Ren, Y., et al. (2020). Highly selective hydrogenation of CO_2 to ethanol via designed bifunctional Ir_1-In_2O_3 single-atom catalyst. *J. Am. Chem. Soc.* 142, 19001–19005. doi: 10.1021/jacs.0c08607

Yoshida, K., Kobayashi, H., Bisaiji, Y., Oikawa, N., and Fukuma, T. (2016). Application and improvement of NO_x storage and reduction technology to meet real driving emissions. *Top. Catal.* 59, 845–853. doi: 10.1007/s11244-016-0558-2

Zhang, Z., Chen, Y., Zhou, L., Chen, C., Han, Z., and Zhang, B., et al. (2019). The simplest construction of single-site catalysts by the synergism of micropore trapping and nitrogen anchoring. *Nat. Commun.* 10:1657. doi: 10.1038/s41467-019-09596-x

Conflict of Interest: The authors declare that the research was conducted in the absence of any commercial or financial relationships that could be construed as a potential conflict of interest.